A Monte Carlo program for photon transport using analogue sampling of scattering angle in coherent and incoherent scattering processes

Jan Persliden

Department of Radiation Physics, Linköping University, The Medical School, S-581 85 Linköping, Sweden

A computer program was developed for the Monte Carlo simulation of photon transport. The program was designed for photon transport simulation in geometries occurring in diagnostic radiology and especially for the investigation of scattered radiation. A method is described for the analogue sampling of scattering angle in coherent and incoherent scattering processes. The two scattering processes are treated separately, and the influence of coherent scattering, an often neglected process, can be estimated quantitatively. The program can also be used for the calculation of the energy imparted to water slabs and fluorescent screens.

Monte Carlo   Photon transport   Incoherent scattering   Coherent scattering

1. INTRODUCTION

The Monte Carlo program described in this paper was developed for the investigation of scattered radiation in diagnostic radiology; its generation in the patient (simulated by water slabs) and subsequent absorption in detectors of varying thicknesses and atomic composition (usually containing elements of high atomic number).

The Monte Carlo method for simulating photon transport was initially applied to neutron–photon radiation shielding problems. The basic principle of the technique was described by Fano, Spencer and Berger [1]. Carter and Cashwell published a review [2] of the Monte Carlo method as applied to particle transport. Reaside [3] cited examples of the Monte Carlo method in medical physics. A recipe for simulating photon transport in X-ray diagnostics was given by Alm Carlsson [4].

Several large computer codes have been developed for general neutron and coupled neutron–photon transport simulations; e.g., MORSE [5], MCNP [6] and TRIPOLI II [7].

The transport program presented in this paper was written for some special applications in diagnostic radiology (i.e., photon energies < 300 keV) and is small and easy to handle.

2. INTERACTION PROCESSES

The geometry in the generation of scattered radiation in the patient or imaging detector etc is illustrated in fig. 1. The X-ray photons enter the medium in a parallel or divergent beam. They may be monoenergetic or polyenergetic. The photons interact with the electrons of the material. The interactions considered are the photoelectric process and the incoherent and coherent scattering processes.

In the photoelectric process the incoming photon is absorbed and a photoelectron emitted. Subsequently, there is emission of low energy Auger electrons and/or characteristic X-ray photons. There is a competition between the occurrence of the two subsequent processes as given by the fluo-
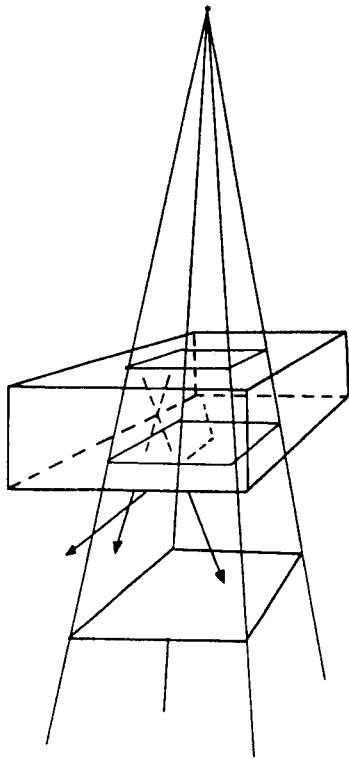
$$S(x, Z)$$

Fig. 1. Geometry used in the Monte Carlo simulation of photon transport in an investigation of scattered radiation. Two singly scattered photon paths and one multiply scattered photon path are illustrated by arrows. The radiation emanates from a point source.

rescence yield. The fluorescence yield for a particular atomic shell is the probability that a characteristic X-ray photon is emitted in filling a vacancy in that shell with an electron from an outer shell. In general, the fluorescence yield is higher the higher the energies of the emitted X-rays. For instance, the K-fluorescence yield in wolfram is 0.96 while it is only 0.036 in aluminium. The photoelectric process is the dominant process in water below a photon energy of 26 keV and below 470 keV in a high atomic number material such as wolfram. A photoelectron having an energy of 300 keV (the maximum energy for the photons considered in the program) has a range of only 0.8 mm in water and can be considered as absorbed at the site of emission. Characteristic X-rays generated in water are of very low energies (< 0.5 keV) and can also be considered to be absorbed at the site of emission. In materials of high atomic number, the

fluorescence yield is so high and the characteristic X-rays are so energetic (e.g., the K_α X-rays in wolfram have a mean energy to 59 keV) that their subsequent transport in the medium has to be considered.

Above 26 keV in water and above 470 keV in wolfram incoherent scattering dominates. Incoherent scattering is a process in which the incident photon transfer energy and momentum to an electron. The photon changes its direction of motion and proceeds with degraded energy. At primary photon energies which are high compared to the electron binding energies, the assumption that the electron is free is a good approximation [8]. The Klein–Nishina differential cross-section valid for free electrons [8] can then be used. At photon energies which are low compared to the electron binding energies, the binding of the electrons to the atom should be considered [8]. The Klein–Nishina differential cross-section per electron is then multiplied by the incoherent scattering function $S(x, Z)$ to obtain the differential incoherent scattering cross-section per atom [8]. Here $x = \sin(\theta/2)/\lambda$, where θ is the scattering angle, λ is the incident photon wave length and Z is the atomic number of the material. The function $S(x, Z)$ increases monotonically from $S(0, Z) = 0$ to $S(\infty, Z) = Z$, [8]. In water, the incoherent scattering cross-section is 97% of the Klein–Nishina cross-section at 60 keV and 72% at 10 keV. In a high atomic number material such as lead, the corresponding figures are 86% and 31% for photons of 100 keV and 10 keV energy, respectively [9].

In coherent scattering, the incident photon changes direction but does not lose appreciable energy since its change of momentum is transferred to the whole atom. Coherent scattering is the dominant scattering process below 13 keV·in $F(x, Z)$ water and below 100 keV in wolfram. The differential scattering cross-section per atom is given by the product of the classical Thompson scattering cross-section per electron and the square of the form factor, $F(x, Z)$, [8] where x and Z have the same meaning as above. The form factor decreases monotonically from $F(0, Z) = Z$ to $F(\infty, Z) = 0$ and consequently the coherent scattering cross-section peaks in the forward direction. The peaking

increases with increasing photon energy and with decreasing atomic number.

3. PROCEDURES FOR SAMPLING COHERENT AND INCOHERENT SCATTERING ANGLE

The sampling of the scattering angle from the appropriate probability distribution is the most crucial step in the Monte Carlo transport program.

It is common to neglect coherent scattering [10]. This may be justified in many situations. However, in diagnostic radiology the neglect of coherent scattering is a poor approximation [11,12].

Efforts have been made to treat the coherent scattering process adequately in Monte Carlo transport calculations in diagnostic radiology:

Dance [13] used the rejection technique (cf. Appendix 2) to sample a scattering angle from the total (incoherent plus coherent) scattering cross-section. After selection of scattering angle, the type of scattering was sampled from the relative frequency of incoherent and coherent scattering at the sampled scattering angle. This method works well above 10 keV for media of low atomic number such as water. However, in materials of higher atomic number or at lower photon energies coherent scattering predominates, and the efficiency of the rejection technique is low. In $CaWO_4$ the efficiency is only 0.3 at 50 keV.

Chen et al. [14] treated incoherent and coherent scattering separately. They sampled from the Klein–Nishina cross-section and the classical Thompson scattering cross-section and corrected for the use of incorrect scattering cross-sections by applying a weight factor to the photon. This method has the disadvantage of impairing the statistical precision of the result, as the weight factors may be large.

Kalender [15] sampled the scattering angle from the total (incoherent plus coherent) scattering cross-section. The range of the scattering angle was then divided into a number of intervals in which the frequency function was approximated

by a linear function. The sampling was then made with the distribution function method (cf. Appendix 3). The energy of the scattered photon was determined from the Compton equation and hence the possibility of a photon being scattered without energy loss was neglected. The program could easily be extended to separate between incoherent and coherent scattering according to the procedure used by Dance [13].

In this work the angles of incoherent and coherent scattering are sampled with a method described by Carter and Cashwell [2]. Both the rejection and the distribution function techniques (see Appendices 2 and 3) are exploited. The sampling is according to the frequency functions (analogue sampling), and weight factors are avoided. For low atomic number material it is as effective as the method of Dance [13] and for materials of high atomic numbers more effective. The scattering processes are treated completely separately from each other, and the effect of coherent scattering can easily be analyzed [16]. The procedures for sampling the scattering angle are treated in detail in section 4.4, the complete program is described in sections 4.1–4.3.

4. COMPUTATIONAL METHODS

4.1. The random number generator

In the sampling procedure true random numbers p should be used. They should be uniformly distributed on the interval [0,1]. Instead of true random numbers, pseudorandom numbers are usually used in computer calculations for practical reasons.

The random number generator used here is a multiplicative, congruential pseudorandom number generator for a 32-bit computer. It is incorporated in the CERN Program Library [17] and has been described by James [18]. The multiplicative factor was changed so that the random number period increased from just over 20×10^6 to over 536×10^6.

The random number generator was tested by

calculating

$$\frac{1}{N} \sum_{i=1}^{N} \rho_i \text{ and } \frac{1}{N} \sum_{i=1}^{N} \rho_i^2.$$

The mean of 10 series with $N = 10^6$ was for

$$\frac{1}{N} \sum_{i=1}^{N} \rho_i \quad 0.4999 \text{ with a standard deviation of } 0.0003$$

and for

$$\frac{1}{N} \sum_{i=1}^{N} \rho_i^2 \quad 0.3325 \text{ with a standard deviation of } 0.0003.$$

The generator passed a χ^2-test, that is, the hypothesis that the random numbers are uniformly distributed could not be rejected on the 0.25 level.

4.2. Interaction cross-section tables

The interaction cross-sections (the total scattering cross-section $\sigma = \sigma_{incoh} + \sigma_{coh}$, the coherent scattering cross-section σ_{coh} and the photoelectric cross-section τ in units of cm^{-1}) were tabulated for each keV from 1–300 keV. The cross-sections for the incoherent scattering were taken from Hubbell et al. [19], for the coherent scattering from Hubbell and Øverbø [20], and for the photoelectric interaction from Storm and Israel [21], and were interpolated exponentially. Cross-sections for the water molecule were obtained by summing the cross-sections for two hydrogen and one oxygen atom.

4.3. The random sampling of photon trajectories

4.3.1. Energy, entrance point and direction of motion for the primary photon

The photon energy is sampled from a known energy spectrum with the rejection technique. Energy spectra covering a range of X-ray tube accelerating potential differences between 40–130 kV were taken from Reiss and Steinle [22]. A coordinate system (the laboratory system) is oriented on the medium in which the photons travel, with the z-axis perpendicular to its surface and pointing

into it. The photons enter the medium either in a parallel beam or in a divergent beam, the central ray in both cases being perpendicular to the medium surface (cf. fig. 1).

A. Parallel beam

The photons can enter the medium in a pencil beam at the origin of the coordinate system ($x = y = z = 0$) or in a rectangular or circular beam.

The coordinates (x, y) of the entrance point in a rectangular field are sampled from two random numbers, ρ_1 and ρ_2, as

$$x = x_{max}(1 - 2\rho_1) \tag{1}$$

$$y = y_{max}(1 - 2\rho_2) \tag{2}$$

$$z = 0 \tag{3}$$

where x_{max} and y_{max} determine the field size.

For a circular field, the distance r from the origin of the coordinate system to the entrance point is determined as:

$$r = r_{max}\sqrt{\rho_1} \tag{4}$$

and the azimuthal angle ϕ as:

$$\phi = 2\pi\rho_2 \tag{5}$$

where ρ_1 and ρ_2 are random numbers and r_{max} the radius of the field.

B. Divergent beam

The photons emerge from a point (isotropically emitting) source at a distance f from the origin of the laboratory coordinate system. The direction of the emitted photon in the laboratory system is given by eq. (6):

$$\vec{\Omega} = (\sin\theta \cos\phi, \sin\theta \sin\phi, \cos\theta) \tag{6}$$

where θ and ϕ are polar and azimuthal angles, respectively.

In most situations a fixed field area (collimated beam) is considered. The frequency function for θ

may then be written:

$$g(\theta) = \frac{\sin\theta \, d\theta}{1 - \cos\theta_{max}} \qquad (7)$$

where θ_{max} is the maximum angle allowed by the field dimensions.

The angle θ is sampled by:

$$\theta = \arccos[1 - \rho(1 - \cos\theta_{max})] \qquad (8)$$

where ρ is a random number. The azimuthal angle ϕ is sampled from eq. (5) and the direction of motion is given by eq. (6).

The value of r, the distance from the origin of the laboratory coordinate system to the entrance point (cf. fig. 2), is:

$$r = f \cdot \tan\theta = f \cdot \tan(\arccos[1 - \rho(1 - \cos\theta_{max})]) \qquad (9)$$

The coordinates of the entrance point can now be calculated.

For a rectangular field, the circular field is extended to the diagonals of the rectangle and the photons entering outside the rectangle are rejected.

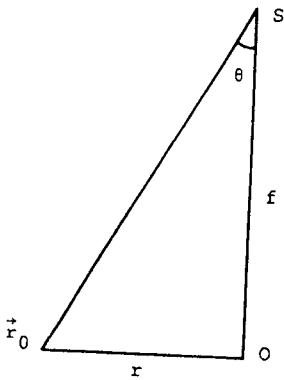The eq. (1–4) and (9) are given for a slab geometry, but can be extended to other media configurations.

Fig. 2. Illustration of the connection between the polar angle θ of the direction of motion and the distance r of the entrance point, $\vec{r}_0$, from the origin, O, of the coordinates in the laboratory system. The photon is emitted from a point source, S, situated at a distance f from O. Slabgeometry.

4.3.2. Pathlength travelled before interaction

After determining the photon energy, its entrance point and direction of motion, the pathlength p travelled before interaction is sampled from the frequency function:

$$f(p) = \mu(h\nu)e^{-\mu(h\nu)p} \qquad (10)$$

Using the distribution function method, a random number ρ is drawn and p is: $0 \leq \xi \leq 1$

$$p = -\ln(\rho)/\mu(h\nu) \qquad (11)$$

where $\mu(h\nu)$ is the linear attenuation coefficient for the material at photon energy $h\nu$. When the pathlength p exceeds the medium thickness d, in the photon's direction, the photon is registered as a transmitted primary photon. A new trajectory is started. If $p < d$, an interaction occurs.

4.3.3. Type of interaction at the interaction point

The type of interaction at a particular photon energy $(h\nu)$ is sampled according to the relative frequency of photoelectric absorption $\tau(h\nu)$, incoherent scattering $\sigma_{inc}(h\nu)$, and coherent scattering $\sigma_{coh}(h\nu)$. A random number ρ is drawn. If:

$$\rho \leq \frac{\tau(h\nu)}{\mu(h\nu)} \qquad (12)$$

a photoelectric absorption occurs.

If:

$$\rho > \frac{\tau(h\nu) + \sigma_{coh}(h\nu)}{\mu(h\nu)} \qquad (13)$$

incoherent scattering occurs;

and if:

$$\frac{\tau(h\nu)}{\mu(h\nu)} < \rho \leq \frac{\tau(h\nu) + \sigma_{coh}(h\nu)}{\mu(h\nu)} \qquad (14)$$

coherent scattering occurs.

In the case of photoelectric absorption, the random walk is terminated and a new one is

started, unless characteristic X-rays are emitted with such high energy that they have to be incorporated into the photon transport. The emission of characteristic X-rays is given by the fluorescence yield, defined in section 2. If a characteristic X-ray is emitted, its direction of motion is given by eq. (6) with the azimuthal angle sampled from eq. (5) and the polar angle sampled from eq. (7) with $\theta_{max} = \pi$. The characteristic X-ray then enters the program in 4.3.2. Auger electrons are considered as absorbed at the site of emission. If a scattering process occurs, values for θ_s (polar angle) and ϕ_s (azimuthal angle) of the scattering are sampled from the appropriate frequency functions; sampling of θ_s is described in section 4.4. and ϕ_s is determined according to eq. (5).

When the scattering is incoherent the energy $h\nu'$ of the scattered photon is taken as the Compton energy:

$$h\nu' = h\nu / \left[1 + (h\nu/m_0c^2)(1 - \cos\theta)\right] \qquad (15)$$

where:

m_0c^2 = the energy equivalence of the electron rest mass (511 keV);

and

θ = the scattering angle.

The small energy broadening of the incoherently scattered photons [12] is thus neglected.

4.3.4. Relation between spatial coordinates of successive interaction points

The sampled scattering angles, θ_s and ϕ_s, are defined with respect to a coordinate system in which the incident photon's direction of motion forms the polar axis. The scattered photon's direction of motion, expressed in the coordinates of the laboratory system, is given by the recurrence formulae (e.g., [4]):

$$\cos\theta_{n+1} = \sin\theta_s \cos\phi_s \sin\theta_n + \cos\theta_s \cos\theta_n \qquad (16)$$

$$\sin(\phi_{n+1} - \phi_n) = -\frac{\sin\theta_s \sin\phi_s}{\sin\theta_{n+1}} \qquad (17)$$

$$\cos(\phi_{n+1} - \phi_n) = \frac{\cos\theta_s - \cos\theta_n \cos\theta_{n+1}}{\sin\theta_n \sin\theta_{n+1}} \qquad (18)$$

where:

θ_n and ϕ_n are the polar and azimuthal angles, respectively, before the n-th scattering and θ_{n+1} and ϕ_{n+1} after. p_{n+1} is the pathlength travelled between the n-th and the $(n + 1)$th interaction and the relationship between the spatial coordinates (x_n, y_n, z_n) and $(x_{n+1}, y_{n+1}, z_{n+1})$ of these interactions is given in the laboratory system by:

$$x_{n+1} = x_n + p_{n+1} \sin\theta_{n+1} \cos\phi_{n+1} \qquad (19)$$

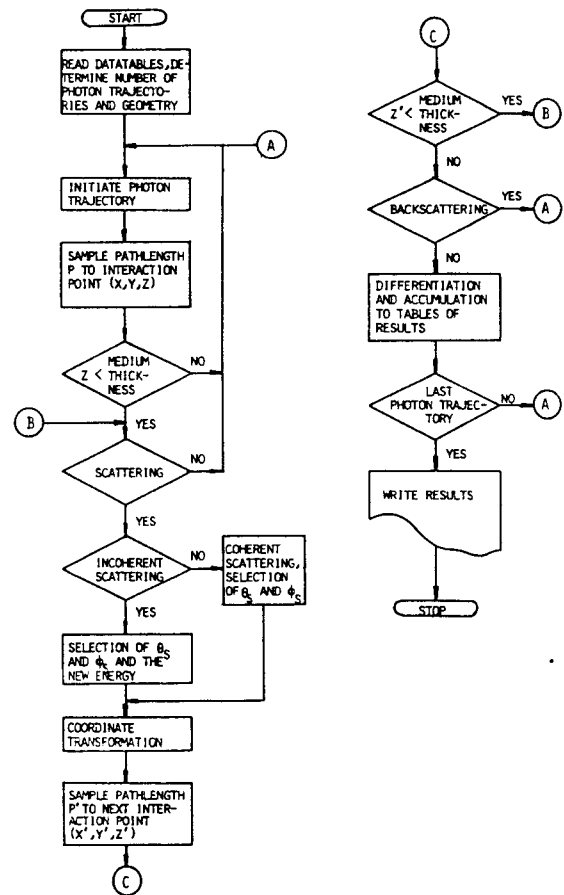$$y_{n+1} = y_n + p_{n+1} \sin\theta_{n+1} \sin\phi_{n+1} \qquad (20)$$

Fig. 3. Flowchart of the main steps in the Monte Carlo program.

$$z_{n+1} = z_n + p_{n+1} \cos \theta_{n+1} \qquad (21)$$

4.3.5 Photon trajectory termination

The photon trajectory is continued until the photon is absorbed or escapes from the medium. In the latter case it is classified according to energy, direction of motion, and spatial coordinates when leaving the medium.

A new trajectory is generated until the predetermined total number of trajectories is reached.

The final result is presented as the plane fluence and the plane energy fluence differential with respect to photon energy, direction of motion, and site of escape. Plane fluence is the number of photons passing per unit area of the slab in the slab geometry. The plane energy fluence is the total energy of the photons passing per unit area (e.g., [23]). The main steps in the program are shown in the flowchart (fig. 3).

4.4. Sampling of scattering angle in incoherent and coherent scattering

4.4.1. Incoherent scattering

The differential atomic cross-section for incoherent scattering in an angle interval $d\theta$ around θ is given by:

$$\frac{d\sigma_{incoh}(h\nu, \theta, Z)}{d\theta} = \frac{d\sigma_{KN}(h\nu, \theta)}{d\theta} \times S(x, Z) \qquad (22)$$

where $d\sigma_{KN}(h\nu, \theta)/d\theta$ is the free electron Klein–Nishina differential cross-section per electron:

$$\frac{d\sigma_{KN}(h\nu, \theta)}{d\theta} = \frac{r_0^2}{2}\left(\frac{h\nu'}{h\nu}\right)^2\left(\frac{h\nu}{h\nu'} + \frac{h\nu'}{h\nu} - \sin^2\theta\right)$$

$$\times 2\pi \sin\theta \qquad (23)$$

with:

r_0 = classical electron radius ($= 2.8 \times 10^{-15}$ m)
$h\nu$ = incident photon energy
$h\nu'$ = Compton scattered photon energy
θ = polar scattering angle in the photon coordinate system

$S(x, Z)$ is the incoherent scattering function [8], the correction for electron binding.

To sample a scattering angle from this distribution one uses a generalization of the rejection method [2]. One normalizes the distribution and writes:

$$\frac{d\sigma_{incoh}(h\nu, \theta, Z)/d\theta}{\sigma_{incoh}(h\nu, Z)}$$

$$= \frac{S_{max}(x, Z)\sigma_{KN}(h\nu)}{\sigma_{incoh}(h\nu)}$$

$$\times \frac{S(x, Z)}{S_{max}(x, Z)} \times \frac{d\sigma_{KN}(h\nu, \theta)/d\theta}{\sigma_{KN}(h\nu)}$$

$$= C(h\nu) \times \frac{S(x, Z)}{S_{max}(x, Z)} \times \frac{d\sigma_{KN}(h\nu, \theta)/d\theta}{\sigma_{KN}(h\nu)}$$

$$(24)$$

where $S_{max}(x, Z)$ is the maximum value of the function $S(x, Z)$. The function is monotonically increasing with increasing x. For a given value of the incident photon energy, this maximum value equals the value $S(x_{max}, Z)$ for $x_{max} = 1/\lambda$,

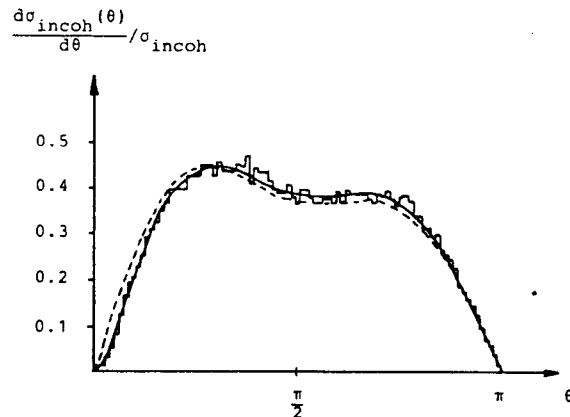Fig. 4. The frequency function $[d\sigma_{incoh}(\theta)/d\theta]/\sigma_{incoh}$ for incoherent scattering of a 50 keV photon in water (solid line). The histogram gives the result of the sampling procedure used in the program based on 100 000 accepted angles. The free electron Klein–Nishina frequency function is given as a dotted line.

($x = \sin(\theta/2)/\lambda$), at $\theta = \pi$. Then, one samples a scattering angle θ from the normalized Klein–Nishina distribution $[d\sigma_{KN}(h\nu, \theta)/d\theta]/\sigma_{KN}(h\nu)$ using the method of Kahn [24] (see Appendix 1). An additional random number ρ is drawn and the value θ for the scattering angle is accepted provided $\rho \leqslant S(x, Z)/S_{max}(x, Z)$; if not the value is rejected and the procedure starts again by sampling from the Klein–Nishina distribution.

The function $S(x, Z)$ is approximated by polynomials of degree 4 or 5 in different x-intervals. In fig. 4 the frequency function $[d\sigma_{incoh}(\theta)/d\theta]/\sigma_{incoh}$ is shown for an incident photon of energy 50 keV in water (solid line). The histogram gives the results of the sampling procedure used in the program based on 100 000 accepted angles. As can be seen, the agreement is good. The free electron $[d\sigma_{KN}(\theta)/d\theta]/\sigma_{KN}$ is also given (dotted line) to demonstrate the influence of the incoherent scattering function $S(x, Z)$.

4.4.2. Coherent scattering

The differential atomic cross-section for coherent scattering is given by:

$$\frac{d\sigma_{coh}(h\nu, \theta, Z)}{d\theta} = \frac{d\sigma_{Th}(\theta)}{d\theta} \times F^2(x, Z) \qquad (25)$$

where $F(x, Z)$ is the atomic form factor and $d\sigma_{Th}(\theta)/d\theta$ is the classical Thompson differential scattering cross-section given by:

$$\frac{d\sigma_{Th}(\theta)}{d\theta} = \frac{r_0^2}{2}(1 + \cos^2\theta)2\pi \sin\theta \qquad (26)$$

The differential cross-section for coherent scattering peaks strongly in the forward direction (small scattering angles θ; cf. fig. 5). The peaking increases with increasing photon energy. The rejection technique in the sample for a scattering angle in coherent scattering becomes inefficient. At this point, a technique with a transformation of variables [2] is used to obtain a more efficient procedure.

The probability that the photon is coherently scattered into the polar angle interval $d\theta$ around θ
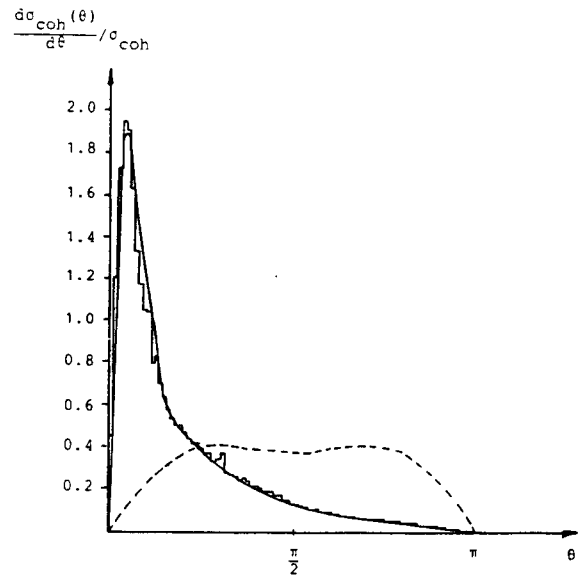

Fig. 5. The frequency function $[d\sigma_{coh}(\theta)/d\theta]/\sigma_{coh}$ for coherent scattering of a 30 keV photon in water (solid line). The histogram gives the result of the sampling procedure used in the program based on 100 000 accepted angles. The frequency function for Thompson scattering is given as a dotted line.

is given by:

$$p(\theta)d\theta = \frac{d\sigma_{coh}(h\nu, \theta, Z)d\theta}{\sigma_{coh}(h\nu, Z)}$$

$$= \frac{r_0^2}{2}\frac{(1 + \cos^2\theta)F^2(x, Z)2\pi \sin\theta d\theta}{\sigma_{coh}(h\nu, Z)}$$

$$(27)$$

The variable θ is exchanged for the variable x^2 where $x = \sin(\theta/2)/\lambda$ and since:

$$\frac{dx^2}{d\theta} = d\left(\frac{\sin(\theta/2)}{\lambda}\right)^2 /d\theta = \sin\theta/2\lambda^2 \qquad (28)$$

one gets:

$$p(x^2)dx^2 = p(\theta)d\theta$$

$$= \frac{r_0^2 \cdot \pi \cdot 2\lambda^2}{\sigma_{coh}(h\nu, Z)}(1 + \cos^2\theta)$$

$$\times F^2(x, Z)dx^2 \qquad (29)$$

One can now introduce the functions:

$$A(x^2, Z) = \int_0^{x^2} F^2(x, Z)\,dx^2 \qquad (30)$$

and

$$A(x_{max}^2, Z) = \int_0^{x_{max}^2} F^2(x, Z)\,dx^2 \qquad (31)$$

where $x_{max} = 1/\lambda$ for $\theta = \pi$.

One may then write $p(x^2)\,dx^2$ as follows:

$$p(x^2)\,dx^2 = \frac{r_0^2 \pi 4\lambda^2 \int_0^{x_{max}^2} F^2(x, Z)\,dx^2}{\sigma_{coh}(h\nu, Z)}$$

$$\times \left(\frac{1 + \cos^2\theta}{2}\right) F^2(x, Z)$$

$$\Big/ \int_0^{x_{max}^2} F^2(x, Z)\,dx^2 \qquad (32)$$

or as:

$$p(x^2)\,dx^2 = C(h\nu, Z) \times g(\theta) \times f(x^2, Z) \qquad (33)$$

Now, $f(x^2, Z)$ is a frequency function and $g(\theta)$ is bounded, $0 \leqslant g(\theta) \leqslant 1$. One samples a value x^2 from the distribution of $f(x^2, Z)$ using the distri-

bution function method, and obtains a value of θ from the relation $x = \sin(\theta/2)/\lambda$. A random number ρ is drawn, and if $\rho < g(\theta)$, θ is accepted as polar scattering angle; if not, another x^2 value is sampled. This is done for a specified atomic number Z, and a specified photon energy $h\nu$. Consequently, $C(h\nu, Z)$ can be considered to be a constant. In fig. 5, the frequency function $[d\sigma_{coh}(\theta)/d\theta]/\sigma_{coh}$ is compared with results obtained using the sampling procedure; here for a photon energy of 30 keV in water. Another advantage of the method, apart from yielding a high sampling efficiency (see table 1), is that for a given atomic number Z the photon energy $h\nu$ and the scattering angle θ can be combined into the single variable $x = \sin(\theta/2)/\lambda$. This means that for each material it is sufficient to calculate the distribution function $f(x^2, Z)$ once and to use it for all photon energies. The distribution function $A(x^2, Z)/A(x_{max}^2, Z)$ is calculated from:

$$A(x^2, Z) = \int_0^{x^2} F^2(x, Z)\,dx^2$$

$$= \int_0^{x^2} F^2(\sqrt{x^2}, Z)\,dx^2$$

$$= \int_0^{t} F^2(\sqrt{t}, Z)\,dt \qquad (34)$$

with numerical integration. The inverse of the

TABLE 1

The efficiency (Eff.) and time for sampling a scattering angle as functions of photon energy

Energy (keV)	Kahn's method		This work			
			Incoherent scattering		Coherent scattering	
	Eff.	Time (ms)	Eff.	Time (ms)	Eff.	Time (ms)
10	0.59	1.12	0.49	2.16	0.40	1.44
20	0.59	1.05	0.53	2.01	0.62	1.07
40	0.59	1.05	0.55	1.92	0.81	0.91
60	0.58	1.13	0.57	1.87	0.88	0.87
100	0.59	1.12	0.58	1.70	0.94	0.83
150	0.59	1.04	0.59	1.66	0.96	0.82
200	0.59	1.11	0.59	1.62	0.97	0.82
300	0.61	1.08	0.61	1.59	0.98	0.81

distribution $A(x^2, Z)/A(x^2_{max}, Z)$ is approximated by polynomials and stored in the program.

4.4.3 Sampling efficiency

The efficiency in accepting a scattering angle is defined as the quotient between the number of accepted angles and the number of sampling trials. The efficiency in sampling scattering angles, using the above procedures, and the time needed to generate an acceptable value for the scattering angle are shown in table 1 as functions of photon energy. The corresponding values with Kahn's method for sampling from the Klein–Nishina differential cross-section are also given.

5. SAMPLE RUN

The first page of the output from the program is shown in fig. 6. Figure 7 shows the first of 10 tables following the first page. The first 5 of the 10 tables give values of plane fluences of scattered photons transmitted through a slab, the 5 following ones present corresponding values of plane energy fluences. The scattered photons transmitted through the slab are divided into 4 groups characterized by the value of the cosine of their angle of emergence with respect to the normal of the slab: 1 (1–0.968), 2 (0.968–0.866), 3 (0.866–0.669), 4 (0.669–0). In each group of 5 tables, the first 4 tables are identical in structure but distinguish between photons in the 4 groups. The values of plane fluences in fig. 7 are for the photons in group 1 and are differentiated with respect to the distance from the center of the incident beam (columns marked 0–1 cm, 1–2 cm and up to 12–13 cm) and with respect to photon energy (rows marked 0–5 keV, 5–10 keV etc.). The values tabulated give values of $\Delta^3 N/\Delta A \Delta h\nu \Delta\Omega$; i.e., give for the intervals of the distance, the photon energy and the direction of motion the number of photons passing per unit area $(\Delta A = \pi r^2_{n+1} - \pi r^2_n)$ and per unit intervals of energy and solid angle, and are given in units of $cm^{-2} \cdot keV^{-1} \cdot sr^{-1}$. The lower rows at each energy interval (fig. 7) give the estimated relative standard deviation for the values obtained. The 14th column marked > 13 gives

MONTE CARLO ANALOG METHOD, SPECTRUM 70 KV

WATERSLAB-THICKNESS=   20. CM

NUMBER OF GENERATED RANDOM WALKS NH=   100000

TOTAL NUMBER OF TRANSM. SCATTERED PHOTONS=   2611

TOTAL NUMBER OF TRANSM. PRIMARY PHOTONS=   651.000

TOTAL TRANSMITTED PRIMARY ENERGY=   33079.586 keV

TOTAL NUMBER OF PHOTOELECTRIC EFFECTS=   77258

TOTAL NUMBER OF INCOHERENT SCATTERING PROC.=   185886

TOTAL NUMBER OF COHERENT SCATTERING PROC.=   32057

Fig. 6. First page of the output from the Monte Carlo program.

the sum of all photons passing at a distance $r > 13$ cm from the center of the beam in units of $keV^{-1} \cdot sr^{-1}$. The last column gives the total number of scattered photons transmitted through the slab in units of $keV^{-1} \cdot sr^{-1}$. The last row, denoted sum, gives the number of photons transmitted irrespective of energy; in units of $cm^{-2} \cdot sr^{-1}$ for the first 13 columns and in units of sr^{-1} for the last two columns. Finally, the fifth table presents values of $\Delta^2 N/\Delta A \Delta h\nu$; i.e., the number of photons transmitted per unit intervals of area and energy irrespective of their directions of motion. When plane energy fluence is considered, as in the last five tables, the photons transmitted are multiplied by their energies. Instead of the number of photons, N, one gets the energy ΔE of the photons. Values of $\Delta^3 E/\Delta A \Delta h\nu \Delta\Omega$ are given in units of $cm^{-2} \cdot sr^{-1}$.

6. ENERGY IMPARTED

The program has been used to estimate the energy imparted [25,26] to water slabs [16], related to the radiation risk to the patient in X-ray examinations [27]. The energy imparted to a medium is easy to obtain by small modifications in the program. All that has to be done is to register the total incident energy of the photons on to the

```
         0-1 CM 1-2-CM 2-3 CM 3-4 CM 4-5 CM 5-6 CM 6-7 CM 7-8 CM 8-9 CM 9-10 CM 10-11  11-12  12-13  )13    SUM
0- 5 KEV .000E+00.000E+00.000E+00.000E+00.000E+00.000E+00.000E+00.000E+00.000E+00.000E+00.000E+00.000E+00.000E+00.000E+00.000E+00
         .0000   .0000   .0000   .0000   .0000   .0000   .0000   .0000   .0000   .0000   .0000   .0000   .0000   .0000   .0000
5-10 KEV .000E+00.000E+00.000E+00.000E+00.000E+00.000E+00.000E+00.000E+00.000E+00.000E+00.000E+00.000E+00.000E+00.000E+00.000E+00
         .0000   .0000   .0000   .0000   .0000   .0000   .0000   .0000   .0000   .0000   .0000   .0000   .0000   .0000   .0000
10-15 KEV.000E+00.000E+00.000E+00.000E+00.000E+00.000E+00.000E+00.000E+00.000E+00.000E+00.000E+00.000E+00.000E+00.000E+00.000E+00
         .0000   .0000   .0000   .0000   .0000   .0000   .0000   .0000   .0000   .0000   .0000   .0000   .0000   .0000   .0000
15-20 KEV.000E+00.000E+00.000E+00.000E+00.000E+00.000E+00.000E+00.000E+00.000E+00.000E+00.000E+00.000E+00.000E+00.000E+00.000E+00
         .0000   .0000   .0000   .0000   .0000   .0000   .0000   .0000   .0000   .0000   .0000   .0000   .0000   .0000   .0000
20-25 KEV.000E+00.000E+00.000E+00.000E+00.000E+00.000E+00.000E+00.000E+00.000E+00.000E+00.000E+00.000E+00.000E+00.000E+00.000E+00
         .0000   .0000   .0000   .0000   .0000   .0000   .0000   .0000   .0000   .0000   .0000   .0000   .0000   .0000   .0000
25-30 KEV.191E+01.000E+00.636E-01.000E+00.000E+00.000E+00.000E+00.000E+00.000E+00.000E+00.000E+00.000E+00.000E+00.000E+00.100E+02
         .4082   .0000  1.0000   .0000   .0000   .0000   .0000   .0000  .212E-01.000E+00.000E+00.000E+00.000E+00.000E+00 .3162
30-35 KEV.700E+01.212E+00.127E+00.273E+00.000E+00.000E+00.000E+00 1.0000 .0000   .0000   .0000   .0000   .0000   .000E+00.430E+02
         .2132   .7071   .7071   .4082   .0000   .0000  .489E-01.000E+00.187E-01.167E-01.152E-01.277E-01.255E-01.000E+00 .1525
35-40 KEV.146E+02.636E+00.127E+00.318E+00.354E-01.289E-01.489E-01.424E-01.936E-01.167E-01.606E-01.138E-01.509E-01.100E+01.890E+02
         .1474   .4082   .7071   .3780  1.0000  1.0000   .7071   .7071   .424E-01...     .5000  1.0000   .5000  1.0000 .1060
40-45 KEV.210E+02.530E+00.255E+00.182E+00.106E+00.578E-01.245E-01.848E-01.374E-01.167E-01.303E-01.138E-01.000E+00.100E+01.106E+03
         .1231   .4472   .5000   .5000   .5774   .7071  1.0000   .5000   .374E-01...    1.0000   .0000  1.0000 .0971
45-50 KEV.207E+02.530E+00.636E-01.000E+00.141E+00.289E-01.489E-01.424E-01.374E-01.000E+00.152E-01.000E+00.000E+00.100E+01.860E+02
         .1240   .4472  1.0000   .0000   .0000  .245E-01.489E-01.424E-01.374E-01.000E+00  1.0000   .0000  1.0000 .1078
50-55 KEV.143E+02.530E+00.191E+00.909E-01.707E-01.000E+00.245E-01.000E+00.000E+00.167E-01.000E+00.000E+00.000E+00.100E+01.590E+02
         .1491   .4472   .5774   .7071   .7071   .0000  .245E-01.000E+00.000E+00.167E-01  1.0000   .0000  .0000 .1302
55-60 KEV.121E+02.318E+00.191E+00.455E-01.354E-01.289E-01.245E-01.000E+00.000E+00.167E-01.000E+00.000E+00.000E+00.000E+00.480E+02
         .1622   .5774   .5774  1.0000  1.0000  1.0000  .245E-01.000E+00.000E+00.000E+00.000E+00.000E+00.000E+00 .1443
60-65 KEV.573E+01.318E+00.000E+00.455E-01.000E+00.000E+00.000E+00.000E+00.000E+00.000E+00.000E+00.000E+00.000E+00.000E+00.220E+02
         .2357   .5774   .0000  1.0000   .0000   .0000   .0000   .0000   .0000   .0000   .0000   .0000   .0000 .2132
65-70 KEV.127E+01.212E+00.636E-01.455E-01.000E+00.000E+00.000E+00.000E+00.000E+00.000E+00.000E+00.000E+00.000E+00.800E+01
         .5000   .7071  1.0000  1.0000   .0000   .0000   .0000   .0000   .0000   .9000   .0000  .0000 .3536
SUM      .493E+03.164E+02.541E+01.500E+01.194E+01.723E+00.110E+01.954E+00.936E+00.335E+00.606E+00.277E+00.382E+00.150E+02.235E+04
         .0568   .1796   .2425   .2132   .3015   .4472   .3333   .3333   .3162   .5000   .3536   .5000   .4082   .5774 .0461
```

Fig. 7. Second page of the output from the Monte Carlo program, giving the first table of results. The table is described in section 5.

slab and to subtract the energies of the transmitted primary photons as well as the energies of the scattered photons escaping from the slab.

7. HARDWARE AND SOFTWARE SPECIFICATIONS

The program is written in FORTRAN IV. The program was run on a SEL 32/77 computer with 32 bits wordlength. It has also been run on a DEC-10. The largest program required 160 kBytes for the SEL computer memory organisation. Another measure of the program's requirements: there is in the largest form 16 matrices to accumulate the results with 1120 real numbers in each. In this form, singly and multiply scattered transmitted photons are separated as well as backscattered photons. The smallest program giving only the transmitted scattered photons requires 96 kByte for the SEL computer. Here 4 matrices of 1120 elements are required. If the plane energy fluence is not needed, the 4 matrices are reduced to 2. In each simulation, tables are read for the cross-section data and for the spectrum used. There are 4 tables with 300 values in each, and for the spectrum 2 tables with a maximum of 390 values are used. The running time is directly dependent on the number of photon trajectories. For 100 000 photon trajectories the running time was 16 min/43 s on the SEL computer.

8. PROGRAM AVAILABILITY

The program is available from the author.

ACKNOWLEDGEMENT

REFERENCES

[1] U. Fano, L.V. Spencer and M.J. Berger, Penetration and diffusion of X-rays, in: Handbuch der Physik. Band 38/2, pp. 660–817, S. Flügge ed. (Springer-Verlag, Berlin, 1959).

[2] L.L. Carter and E.D. Cashwell, Particle-transport simulation with the Monte Carlo method, ERDA Critical Review Series, TID-26607 (USERDA Technical Information Center, Oak Ridge, TN, 1975).

[3] D.E. Reaside, Monte Carlo principles and applications, Phys. Med. Biol. 21 (1976) 181–197.

[4] G. Alm Carlsson, Effective use of Monte Carlo methods for simulating photon transport with special reference to slab penetration problems in X-ray diagnostics, Report ULi-RAD-R-049 (ISSN 0348-7679), 1981.

[5] M.B. Emmett, The MORSE Monte Carlo radiation transport code system, ORNL-4972 (1975).

[6] W.L. Thompson, MCNP – A general Monte Carlo code for neutron and photon transport, LA-8176-MS (1979).

[7] A. Baur, L. Bourdet, G. Dejonghe, L. Gonnord, A. Monnier, J.C. Nimal and T. Vergnaud, Overview on TRIPOLI II, in: A review of the theory and application of Monte Carlo methods, Proceedings of a Seminar Workshop, pp. 313–328, D.K. Trubey et al. eds. ORNL-RSIC-44 (USERDA, Oak Ridge TN, 1980).

[8] W.J. Veigele, P.T. Tracy and E.M. Henry: Compton effect and electron binding, Am. J. Phys. 34 (1966) 1116–1121.

[9] R. Ribberfors, X-ray incoherent scattering total cross sections and energy-absorption cross sections by means of simple calculation routines. Phys. Rev. A 27 (1983) 3061–3070.

[10] S.M. Seltzer, Calculated response of intrinsic Germanium detectors to narrow beams of photons with energies up to ~ 300 keV, Nucl. Instr. Methods 188 (1981) 133–151.

[11] T. Grönberg and S. Mattsson, Monte Carlo determinations of optimal photon energies for XRF analysis of iodine in vivo, Adv. X-ray Anal. 24 (1981) 371–376.

[12] G. Alm Carlsson, C.A. Carlsson, K-F. Berggren and R. Ribberfors, Calculation of scattering cross-sections for increased accuracy in diagnostic radiology: I. Energy

broadening of Compton scattered photons, Med. Phys. 9 (1982) 868–879.

[13] D.R. Dance, The Monte Carlo calculation of integral radiation dose in xeromammography, Phys. Med. Biol. 25 (1980) 25–37.

[14] C.S. Chen, K. Doi, C. Vyborny, H-P. Chan and G. Holje, Monte Carlo simulation studies of detectors used in the measurement of diagnostic X-ray spectra, Med. Phys. 7 (1980) 627–635.

[15] W.A. Kalender, Determination of the intensity of scattered radiation and the performance of grids in diagnostic radiology by Monte Carlo methods (Thesis, Univ. of Wisconsin, Madison WI, 1979).

[16] J. Persliden and G. Alm Carlsson (1983) submitted.

[17] CERN Program Library, Program Library, Division DD, CERN (1211 Geneva 23, 1980).

[18] F. James, Monte Carlo Theory and Practice. Rep. Prog. Phys. 43 (1980) 1145–1189.

[19] J.H. Hubbell, W.J. Veigele, E.A. Briggs, R.T. Brown, D.T. Cromer and R.J. Howerton, Atomic Form Factors, Incoherent Scattering Functions and Photon Scattering Cross Sections, J. Phys. Chem. Ref. Data 4 (1975) 471–538.

[20] J.H. Hubbell and I. Øverbø, Relativistic Atomic Form Factors and Photon Coherent Scattering Cross Sections, J. Phys. Chem. Ref. Data 8 (1979) 69–105.

[21] E. Storm and H.I. Israel, Photon Cross Sections from 1 keV to 100 MeV for Elements $Z = 1$ to $Z = 100$. Nuclear Data Tables 7 (1970) 565–681.

[22] K.A. Reiss and B. Steinle, Tabellen zur Röntgendiagnostik. II. (Siemens A.G., Erlangen, 1973).

[23] C.A. Carlsson, Relationships between energy fluence and energy incident on, emitted by or imparted to a body, Phys. Med. Biol. 24 (1979) 1209–1215.

[24] H. Kahn, Applications of Monte Carlo, RM-1237-AEC (Rand Corp., Santa Monica CA, 1956).

[25] ICRU, Radiation Quantities and Units, ICRU Report 33. (Int. Comm. Radiation Units and Measurements, Washington DC, 1980).

[26] G. Alm Carlsson and C.A. Carlsson, Quantities and Concepts Used in Radiation Dosimetry. Int. J. Appl. Radiat. Isotopes 33 (1982) 953–965.

[27] C.A. Carlsson, Information sampling in diagnosis with minimal radiation risk to patients, in: Proc. Int. School of Physics 'Enrico Fermi' Course LXXVI Medical Physics, pp. 481–490, J.R. Greening, ed. (Elsevier/North-Holland, Amsterdam, New York NY, 1981).

APPENDIX 1

Kahn's method of sampling scattered photon energy from the free-electron Klein–Nishina distribution

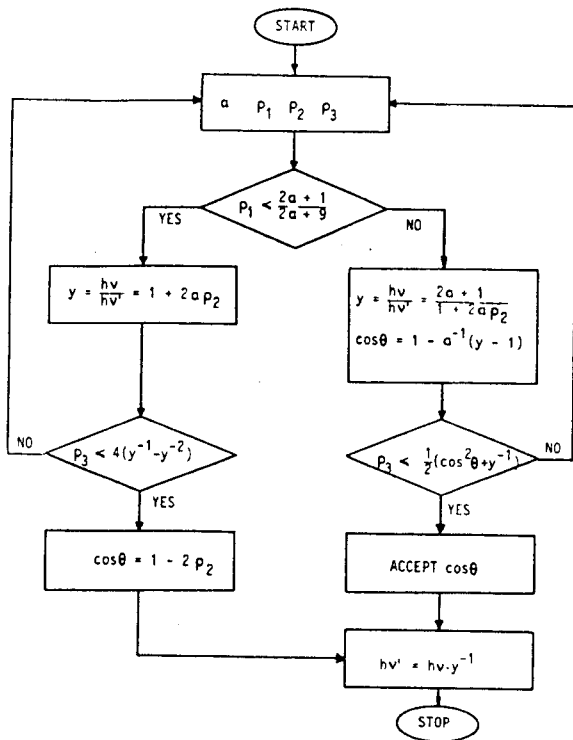Kahn's method [24] of sampling a scattered photon energy $h\nu'$ from the free electron

Fig. A1. Flow-chart of Kahn's method of sampling scattered photon energy from the Klein–Nishina differential scattering cross-section.

Klein–Nishina differential scattering cross-section is described without proof in the flowchart shown in fig. A1.

Notations: $\alpha = h\nu/m_0 c^2$, where $h\nu$ is the incident photon energy and $m_0 c^2$ is the energy equivalent of the electron rest mass. Three random numbers ρ_1, ρ_2 and ρ_3 must be used.

APPENDIX 2

The rejection method

When sampling a value x_1 from a given frequency function $f(x)$ the rejection technique can be used (for details, see [2,4]).

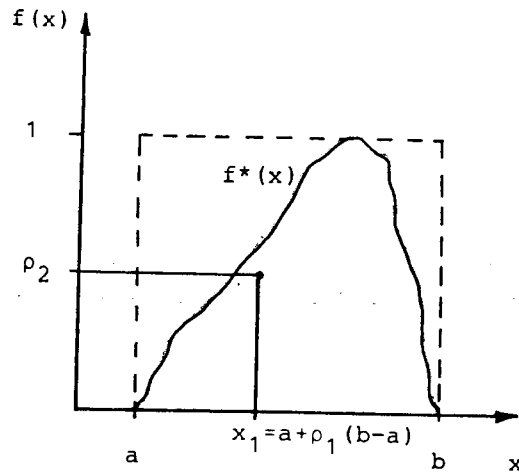Let $f(x)$ be a bounded frequency function on the

Fig. A2. Illustration of the rejection technique of sampling from the frequency function $f(x)$ using two random numbers ρ_1 and ρ_2.

interval $[a,b]$:

$$f^*(x) = \frac{f(x)}{\sup f(x)} \qquad (A2.1)$$

where

$$\int_a^b f(x)\,\mathrm{d}x = 1 \qquad (A2.2)$$

and $\sup f(x)$ is the maximum value of the function $f(x)$.

Draw two random numbers ρ_1 and ρ_2. Calculate:

$$x_1 = a + \rho_1(b - a) \qquad (A2.3)$$

If

$$\rho_2 \leqslant f^*(x_1) \qquad (A2.4)$$

x_1 can be accepted as a sample value; if not, x_1 is rejected. The method is illustrated in fig. A2. The sampling efficiency (section 4.4.3) is given by:

$$
\begin{aligned}
\text{Sampling efficiency} &= \frac{\int_a^b f^*(x)\,\mathrm{d}x}{(b-a)} \\
&= \frac{\int_a^b \dfrac{f(x)}{\sup f(x)}\,\mathrm{d}x}{(b-a)} \\
&= \frac{1}{(b-a)\,\sup f(x)} \qquad (A2.5)
\end{aligned}
$$

APPENDIX 3

The distribution function method

Sampling from a normalized frequency function $f(x)$, where the inverse of the distribution function is obtainable, can be performed using the distribution function method. The case with a continuous frequency function $f(x)$ will be considered.

Let $f(x)$ be a continuous normalized frequency function on the interval $[a,b]$. The distribution function $F(x)$ is then:

$$F(x) = \int_a^x f(x') dx' \qquad (A3.1)$$

Drawing a random number ρ and making:

$$F(x) = \rho \qquad (A3.2)$$

yields

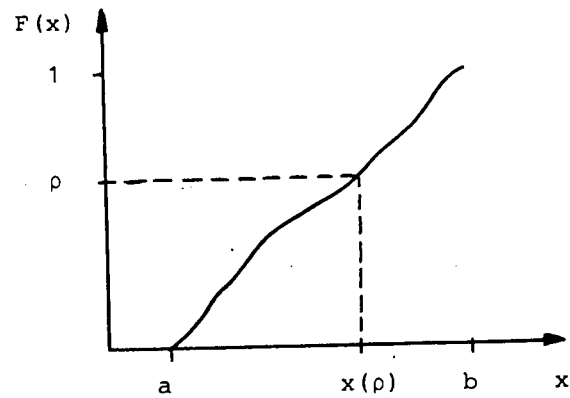$$x = F^{-1}(\rho) \qquad (A3.3)$$

Fig. A3. Illustration of the distribution function method of sampling from the frequency function $f(x)$ using one random number ρ.

where F^{-1} is the inverse of F. The method is illustrated in fig. A3 above. The efficiency of this method is 1, because each random number gives an accepted value.